3-28-2015

Thermal boundary conditions on western Greenland: Observational constraints and impacts on the modeled thermomechanical state

Toby W. Meierbachtol
University of Montana - Missoula

Joel T. Harper
University of Montana - Missoula, joel.harper@mso.umt.edu

Jesse V. Johnson
University of Montana - Missoula

Neil F. Humphrey
University of Wyoming

Douglas John Brinkerhoff
University of Montana - Missoula, douglas.brinkerhoff@umontana.edu

Recommended Citation

Meierbachtol, T. W., J. T. Harper, J. V. Johnson, N. F. Humphrey, and D. J. Brinkerhoff (2015), Thermal boundary conditions on western Greenland: Observational constraints and impacts on the modeled thermomechanical state, J. Geophys. Res. Earth Surf., 120, 623–636, doi:10.1002/2014JF003375.

AGU PUBLICATIONS

JGR

Journal of Geophysical Research: Earth Surface

RESEARCH ARTICLE
10.1002/2014JF003375

Key Points:
- Measured thermal boundaries differ from commonly used data sets
- Observation-driven basal heat flux increases numerical model cold bias
- Surface temperature adjustments impact modeled thermal behavior at depth

Correspondence to:
T. W. Meierbachtol,
toby.meierbachtol@umontana.edu

Citation:
Meierbachtol, T. W., J. T. Harper, J. V. Johnson, N. F. Humphrey, and D. J. Brinkerhoff (2015), Thermal boundary conditions on western Greenland: Observational constraints and impacts on the modeled thermomechanical state, *J. Geophys. Res. Earth Surf.*, *120*, 623–636, doi:10.1002/2014JF003375.

Received 24 OCT 2014
Accepted 21 JAN 2015
Accepted article online 26 JAN 2015
Published online 28 MAR 2015

Thermal boundary conditions on western Greenland: Observational constraints and impacts on the modeled thermomechanical state

Toby W. Meierbachtol[1], Joel T. Harper[1], Jesse V. Johnson[2], Neil F. Humphrey[3], and Douglas J. Brinkerhoff[2,4]

[1]Department of Geosciences, University of Montana, Missoula, Montana, USA, [2]Department of Computer Science, University of Montana, Missoula, Montana, USA, [3]Department of Geology and Geophysics, University of Wyoming, Laramie, Wyoming, USA, [4]Department of Geology and Geophysics, University of Alaska Fairbanks, Fairbanks, Alaska, USA

Abstract The surface and basal boundary conditions exert an important control on the thermodynamic state of the Greenland Ice Sheet, but their representation in numerical ice sheet models is poorly constrained due to the lack of observations. Here we investigate a land-terminating sector of western Greenland and (1) quantify differences between new observations and commonly used boundary condition data sets and (2) demonstrate the impact of improved boundary conditions on simulated thermodynamics in a higher-order numerical flow model. We constrain near-surface temperature with measurements from two 20 m boreholes in the ablation zone and 10 m firn temperature from the percolation zone. We constrain basal heat flux using in situ measurement in a deep bedrock hole at the study area margin and other existing assessments. To assess boundary condition influences on simulated thermal-mechanical processes, we compare model output to multiple full-thickness temperature profiles collected in the ablation zone. Our observation-constrained basal heat flux is 30 mW m^{-2} less than commonly used representations. In contrast, measured near-surface temperatures are warmer than common surface temperature data sets by up to 15°C. Application of lower basal heat flux increases a model cold bias compared to the measured temperature profiles and causes frozen basal conditions across the ablation zone. Temperate basal conditions are reestablished by our warmer surface boundary. Warmer surface ice and firn can introduce several times more energy to the modeled ice mass than what is lost at the bed from reduced basal heat flux, indicating that the thermomechanical state of the ice sheet is highly sensitive to near-surface effects.

1. Introduction

The need to constrain mass balance and ice flow changes in coming centuries has motivated substantial improvements to deterministic models of the Greenland Ice Sheet (GrIS). Higher-order physics have been adopted [e.g., *Larour et al.*, 2012; *Brinkerhoff and Johnson*, 2013], surface and bed geometry are more highly resolved [*Bamber et al.*, 2013], and surface velocity fields now provide spatial coverage at a sufficient level to provide a target for model tuning at the full ice sheet scale [*Joughin et al.*, 2010; *Rignot and Mouginot*, 2012]. Yet despite these advances, the upper and lower thermal boundaries of the ice sheet remain poorly constrained by direct observations. These boundary conditions dictate the thermal state of the ice sheet and therefore are primary controls on internal deformation and the basal conditions which govern sliding.

The thermal surface boundary condition in ice flow models is typically prescribed as the snow/ice temperature at a shallow depth where seasonal variations are damped. On the GrIS, observations in the near-surface layer (~10 m depth) are limited to a number of point measurements, many of them only sporadic [*Benson*, 1962; *Mock and Weeks*, 1965; *Echelmeyer et al.*, 1992; *Humphrey et al.*, 2012; *Koenig et al.*, 2014]. Such sparse measurements have required that the surface boundary be defined by surface temperature output from regional climate models (RCMs). Yet the assumption that the mean annual surface temperature is equivalent to the temperature at shallow depth is only valid on the GrIS at high elevations in the dry snow zone [*Mock and Weeks*, 1965] and fails in the lower glacier facies.

Latent heat release from the refreezing of percolating meltwater raises near surface temperatures by up to 10°C above the annual surface mean in the percolation zone [*Humphrey et al.*, 2012]. In the ablation zone,

insulation from winter accumulation and subsequent latent heat release from refreezing of spring melt provide heat sources, while the inability of the ice temperature to rise above 0°C in the summer months induces an apparent cooling effect [*Hooke et al*., 1983]. Air-filled crevasses and moulins exert additional thermal influences which can either cool by cold air conduction [*Echelmeyer et al*., 1992] or heat by solar radiation absorption [*Pfeffer and Bretherton*, 1987]. Water-filled crevasses, moulins, and other macroscale hydrologic features provide a substantial heat reservoir that can contribute to near-surface or full-thickness warming for multiple years [*Jarvis and Clarke*, 1974; *Phillips et al*., 2010].

At the basal boundary for energy conservation, direct measurement of geothermal heat flux (GHF) has, until recently, been limited to two sites in southern GrIS [*Sass et al*., 1972]. Indirect model-based studies utilizing ice core temperature records [*Dahl-Jensen et al*., 1998; *Petrunin et al*., 2013] have increased direct and indirect heat flux measurements to four point locations across the 1.71 million square kilometer (km^2) ice sheet. Due to the lack of direct measurements, maps of heat flux at the ice sheet scale are commonly utilized. These spatially variable fields are generated from satellite-derived magnetic crustal thickness [*Fox Maule et al*., 2009] or extrapolation of the global heat flux data set based on tectonic [*Pollack et al*., 1993] or seismic models [*Shapiro and Ritzwoller*, 2004]. However, these maps exhibit little consistency between one another or with independent observations. In fact, a uniform heat flow produces a better model match to measured ice core temperatures than any of the spatially variable models [*Rogozhina et al*., 2012].

The paucity of data constraining Greenland's thermal boundaries forces ice sheet modeling studies to employ boundary condition data sets which are inconsistent at the bed and neglect critical warming and cooling processes at the surface. The resulting thermomechanical behavior is unlikely to reflect the current state of the GrIS, but assessment of modeled thermal biases is hindered by the lack of metrics away from the ice sheet divide [*Rogozhina et al*., 2012; *Seroussi et al*., 2013]. Thus, the thermal state of the ice sheet remains subject to considerable uncertainty, motivating the work here. In this study we focus on a $>$14,000 km^2 region of western Greenland where recent ice and bedrock borehole studies provide thermal constraints. We augment near-surface ice temperature and direct measurement of bedrock heat flux from these field campaigns with additional in situ observations to quantify the differences between data sets commonly used in ice flow models and our observation-constrained boundary conditions. We then test the thermal sensitivity of a higher-order numerical ice sheet model to switching between existing boundary data sets and our adjusted boundaries, using full-thickness temperature measurements collected in a transect of deep boreholes through the ablation zone as observational metrics to assess model biases.

2. Methods

2.1. Study Area

We focus the study on a subsection of the western GrIS extending east from Isunnguata Sermia (IS), a land terminating outlet glacier, to the ice sheet divide (Figure 1). This region of the ice sheet is uniquely constrained by field data due to closely gridded airborne radar captured through the ICEBRIDGE project [*Allen et al*., 2010], multiple in situ ice temperature measurements from a recent ice borehole drilling campaign [*Meierbachtol et al*., 2013; *Harrington et al*., 2015], and temperatures in a deep bedrock borehole at the ice sheet margin [*Harper et al*., 2010].

2.2. Data

2.2.1. Near-Surface Temperature

During the 2011 field campaign we drilled 20 m boreholes at two sites below the equilibrium line altitude (ELA) using hot water methods and instrumented these holes with data logging thermistor strings (Figure 1). Instrument strings consisted of 32 temperature sensors spaced at 0.6 m intervals to a maximum depth of 20 m below the surface and captured measurements at 1 to 3 h intervals. Temperature time series in the holes show the thermal disturbance from drilling is effectively eliminated within 2–3 weeks of drilling. The thermistor strings and data loggers were identical to those used by *Humphrey et al*. [2012]. We performed a zero-point calibration in the field and conservatively estimate the accuracy at 1.0°C. To account for large changes in surface elevation associated with seasonal ablation (approaching 3 m a^{-1}), we adjust sensor depth below the ice surface using acoustic depth rangers from on-ice met stations at each site. Temperatures

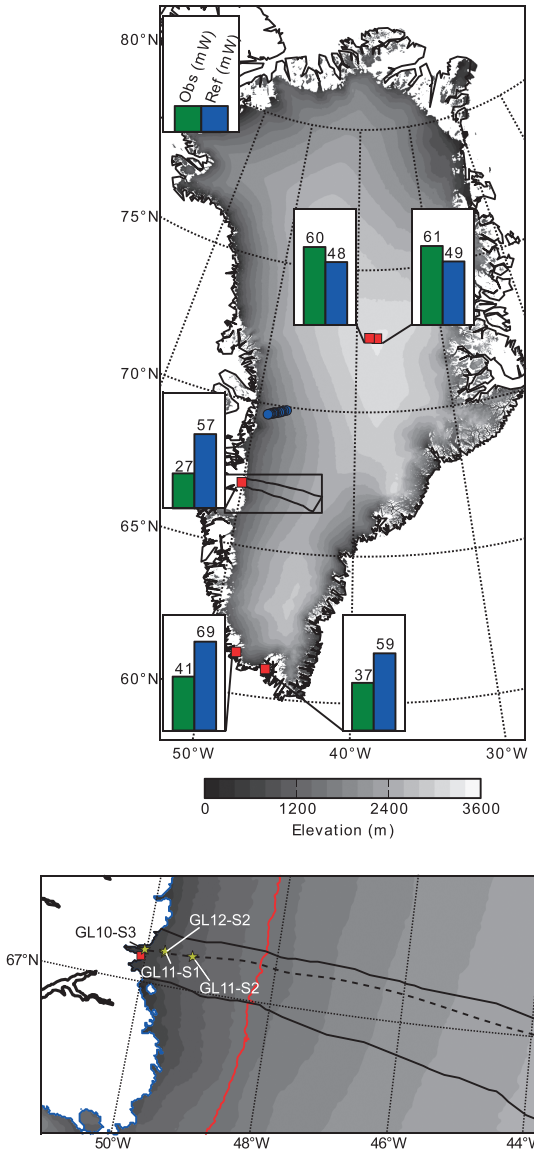

Figure 1. Study area in the context of the Greenland Ice Sheet. Model domain is outlined by the solid black line. Red squares show locations of geothermal heat flux measurements. Blue circles show locations of 10 m firn temperatures used for surface temperature adjustments. Bar charts display a comparison of *Shapiro and Ritzwoller* [2004] modeled geothermal heat flux (blue) against available direct and indirect measurements of heat flux (green), with heat flux values given in mW m^{-2}. Yellow stars in the inset show the locations of boreholes drilled during the 2010–2012 field seasons. Red line in the inset outlines the approximate ELA at 1550 m elevation. Dashed line in the inset shows the profile transect upon which Figure 7 is based. Surface elevation field is from *Bamber et al.* [2013].

are then binned in 0.6 m increments. We report temperatures measured over a 15 month period from July 2011 to October 2013 at site GL11-S1. At the upper site, GL11-S2, instrument malfunction resulted in a 5 month measurement record from July 2011 to December 2011.

Above the ELA, near-surface temperature measurements are sparse. Measurement availability in central western Greenland was limited to a few measurements below 2000 m in previous efforts by *Reeh* [1991] to parameterize warming in the percolation zone. Since that study, near-surface (10 m) temperatures were measured at 14 sites between 2007 and 2009 along a transect extending inland from Swiss Camp, approximately 270 km north of our study area [*Humphrey et al.*, 2012]. We utilize these measurements to parameterize warming effects above the ELA in our study region.

2.2.2. Geothermal Heat Flux

We constrain our study region's GHF by synthesizing existing observations from other studies. These include direct measurements in bedrock boreholes and indirect measurements utilizing ice core temperatures (Figure 1). Through coupling of lithospheric and ice sheet models, *Petrunin et al.* [2013] found, respectively, that GHF values of approximately 60 and 61 mW m^{-2} resulted in close agreement with measured temperature profiles at GISP2 and GRIP to the north of our model domain. Heat flux from temperature gradients in deep bedrock boreholes at two sites in southern Greenland ranges from 37 to 41.8 mW m^{-2} [*Sass et al.*, 1972]. A >300 m deep bedrock borehole was recently drilled adjacent to our model domain as part of the Greenland Analogue Project (GAP) [*Harper et al.*, 2010]. Temperature gradients in this hole yield a GHF value of 34.8 mW m^{-2}. In 2011 an additional 700 m bedrock hole, terminating under the ice sheet in our model domain, was drilled as part of the same project. Measurements in this hole indicate a GHF of 27.2 mW m^{-2} (L. Claesson Liljedahl et al., in preparation). We use in our analysis the lower GHF value from the deeper hole since it terminates under the ice sheet, but note that using the higher or mean of the two measurements has little effect on our modeling results and interpretation, as both are much lower than standard maps.

Table 1. Parameterization Guidelines for the Thermal Surface Boundary Condition Based on Measurements

E_{mod}[a] > E_{ELA}	($E_{mod} - E_{ELA}$) > E_{peak}[b]	($E_{mod} - E_{ELA}$) > E_{min}[c]	dT[d]
True	True	-	$dT = 80.56 \exp(-3.86 \times 10^{-3}(E_{mod} - E_{ELA}))$
True	False	-	$dT = 3.15 \times 10^{-2}(E_{mod} - E_{ELA})$
False	-	True	$dT = 1.81 \times 10^{-5}(E_{mod} - E_{ELA})^2 - 3.79 \times 10^{-3}(E_{mod} - E_{ELA})$
False	-	False	$dT = 10.1$

[a] E_{mod} is model surface elevation.
[b] E_{peak} is the elevation of peak temperature deviation taken from the temperature measurements in the percolation zone (Figure 5).
[c] E_{min} is the elevation of site GL11-S1. The resulting temperature deviation from the reference data set is given by dT.
[d] Units in °C.

2.2.3. Full-Thickness Temperature Profiles

In addition to measurements near the ice surface (section 2.2.1), we measured temperature at three sites through the full ice thickness during our field campaign. A temperature profile at a fourth site extends to the bottom of a borehole which failed to reach the bed. For a detailed description of methods regarding drilling and temperature measurement at these sites, we direct the reader to *Meierbachtol et al.* [2013] and *Harrington et al.* [2015], respectively.

2.3. Thermal Boundary Conditions

2.3.1. Reference Boundary Data Sets

To maintain consistency with previous modeling investigations, we choose thermal boundary condition data sets provided by the Sea-level Response to Ice Sheet Evolution (SeaRISE) project as reference data sets (http://websrv.cs.umt.edu/isis/index.php/Data). The SeaRISE repository offers seismic- and magnetic-based geothermal heat flux data sets [*Shapiro and Ritzwoller*, 2004; *Fox Maule et al.*, 2009]. We choose the seismic-based data set as these heat flux values (56–65 mW m^{-2} across the study area) generally constitute the lowest values of the various models common to the GrIS. Because our measurement-derived GHF field is lower than this reference data set (see section 3), interpretations based on this comparison are also valid with respect to warmer GHF products. The reference surface boundary condition is defined by the Regional Climate Model (RCM) RACMO mean annual surface temperature, which is temporally averaged over the period 1958–2007 [*Ettema et al.*, 2009]. RACMO output represents temperature at the ice/snow surface, preventing temperatures from warming above 0°C. Both surface and basal thermal boundary data sets are provided at 5 km resolution, which we linearly interpolate over our model domain.

2.3.2. Observation-Based Boundary Parameterization

We compare standard boundary condition data sets with thermal boundary fields which we develop directly from measurements on the ice sheet. Doing so allows us to (1) take advantage of the dense network of observations near our study area (compared to the rest of the GrIS) and (2) treat surface boundary condition changes across changing glacier facies.

We parameterize the surface boundary temperature as an anomaly from the reference data set to preserve larger-scale lapse rates and climatology embedded within the reference RCM. Temperature adjustments follow a heuristic, multipart fit to honor the near-surface measurements. In order to effectively treat the difference in ELA position between the sites along the EGIG line (estimated at 1100 m, near Swiss Camp [*Box et al.*, 2006]) and our study domain (~1550 m [*van de Wal et al.*, 2008]), we use the ELA as a reference elevation and base the parameterization on the elevation above or below this reference point. Above the elevation of maximum temperature deviation in the percolation zone, differences between measured and reference temperatures are fit using an exponential function. Between the ELA and elevation of maximum deviation, the temperature difference between measured and the reference data set follows a linear fit, assuming that the temperature deviation $dT = 0^{\circ}$C at the ELA.

Below the ELA we calculate the difference between our temperature measurements at depth and the reference temperature data set and extrapolate this difference across the ablation zone using a second-order polynomial from the ELA to the elevation of measurement site GL11-S1 (see Figure 1). Below this elevation, we maintain a constant temperature deviation to avoid imposing temperatures greater than 0°C. The parameterization of near-surface temperature across the entire domain is summarized in Table 1.

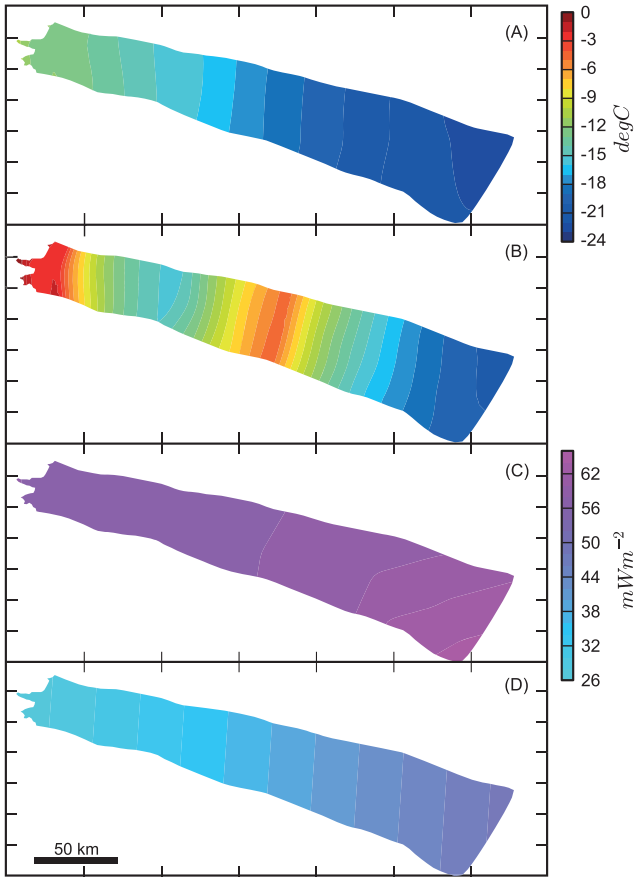

Figure 2. Reference boundary conditions from the SeaRISE project (a and c) and observation-driven boundary conditions (b and d). Surface boundary temperatures are shown in (a) and (b), and geothermal heat flux fields are displayed in (c) and (d).

We distribute GHF from the five-point locations across the model domain through linear interpolation (Figure 2).

2.4. Ice Sheet Model

We implement numerical experiments using the Variational Glacier Simulator (VarGlaS) modeling framework. VarGlaS provides capabilities for three-dimensional modeling of ice flow using finite elements under the premise of the variational principle for the momentum balance [*Brinkerhoff and Johnson*, 2013]. The momentum balance satisfies the Blatter-Pattyn first-order equations [*Blatter*, 1995; *Pattyn*, 2003], which assumes small bed slopes and negligible horizontal gradients in vertical velocity. Thermomechanical coupling is achieved using an enthalpy scheme [*Aschwanden et al.*, 2012]. A complete description of the model formulation and numerics therein can be found in *Brinkerhoff and Johnson* [2013].

The surface boundary of the momentum balance is stress-free, while the basal boundary employs a linear, Weertman-type sliding law with an impenetrability constraint. Zero gradients in stress are implied across the lateral boundaries and at the divide.

The surface boundary in the enthalpy scheme is a prescribed Dirichlet condition representing the mean annual near-surface temperature. Basal gradients in internal energy at the bed are a function of frictional heat generation (following the Weertman-type sliding law), geothermal heat flux, and basal melting respectively:

$$\kappa(H)\nabla H \cdot \mathbf{n} = h\beta^2 \mathbf{u_B} \cdot \mathbf{u_B} + q_{\text{geo}} - M_b \rho L \tag{1}$$

where $\kappa(H)$ is an enthalpy-dependent diffusivity, H is enthalpy, h is ice thickness, β^2 is a tuned basal traction parameter, $\mathbf{u_B}$ is the bed-parallel basal velocity vector, q_{geo} is geothermal heat flux, M_b is the basal melt rate, ρ the density of ice, and L is the latent heat of fusion for water. A natural boundary along the lateral edges in the enthalpy formulation imposes an insulation condition (e.g., $\kappa(H)\nabla H \cdot \mathbf{n} = 0$). At the ice sheet divide, we impose an idealized temperature profile assuming a constant vertical strain rate [*Cuffey and Patterson*, 2010], and accumulation rate of 0.3 m a^{-1} based on available Greenland Climate Network accumulation data [*Steffen et al.*, 1996].

A strength of the Variational Glacier Simulator (VarGlaS) framework is the ability to assimilate observed surface velocities through adjoint-based techniques, which we use to find a steady state instance of the model. The assimilation process minimizes the logarithmic misfit between observed and modeled velocities, subject to the forward model constraint, through the manipulation of the basal traction parameter β^2. We choose a logarithmic cost functional to equitably distribute optimization effort across the full range of velocity magnitudes and address overfitting by imposing a Tikhonov regularization term which penalizes gradients in basal traction [*Gillet-Chaulet et al.*, 2012; *Seroussi et al.*, 2013]. The degree of regularization is a function of the ice sheet thickness

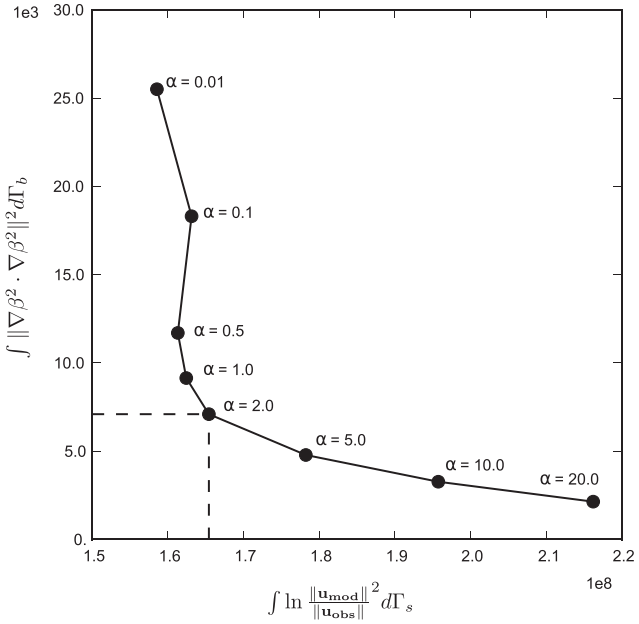

Figure 3. Results from the *L* curve analysis used to constrain the regularization parameter α. A break in slope occurs at $\alpha = 2.0$, representing a reasonable compromise between the model norm $\left(\int_{\Gamma_b} \|\nabla\beta^2 \cdot \nabla\beta^2\|^2 d\Gamma\right)$ and misfit norm $\left(\int_{\Gamma_s} \ln \frac{\|\mathbf{u_{mod}}\|^2}{\|\mathbf{u_{obs}}\|} d\Gamma\right)$.

and the tunable parameter α. This results in the following objective function to be minimized via a Quasi-Newton BFGS scheme [*Nocedal and Wright*, 2000]:

$$I = \int_{\Gamma_s} \left(\ln \frac{\|\mathbf{u_{mod}}\|}{\|\mathbf{u_{obs}}\|} \right)^2 d\Gamma + \alpha h \int_{\Gamma_b} \nabla\beta^2 \cdot \nabla\beta^2 d\Gamma \quad (2)$$

where $\mathbf{u_{mod}}$ and $\mathbf{u_{obs}}$ are modeled and observed surface velocities, respectively. Through the use of an *L* curve analysis [*Aster et al*., 2005], we choose $\alpha = 2$ (Figure 3). Experimentation with different degrees of regularization influences the velocity misfit but does not affect comparison between experiments as described below. With the regularization parameter in hand, we iteratively update the momentum balance through variations in the basal traction parameter β^2 under constant viscosity and enthalpy, calculated from an initial steady state solution. Enthalpy and nonlinear viscosity are updated every 50 iterations during the inversion process. Termination of the inversion is largely a qualitative process, previously referred to as the "recent improvement threshold" approach [*Habermann et al*., 2012]. Under this approach, we terminate the inversion when changes in the objective function between iterations become small.

In model experiments we define the domain by extending 15–20 km north and south of the IS terminus. Lateral boundaries follow the ice sheet surface slope to the divide, closing the domain. Constraining the domain in this way focuses on reaches with dense observation while still allowing transverse gradients throughout the domain (in contrast to two-dimensional flowline modeling). The model surface and bedrock topography are defined by a 1 km digital elevation model (DEM) [*Bamber et al*., 2013]. We apply a Gaussian filter to the surface topography to eliminate locally sharp changes in elevation, which we consider justified as the DEM is constructed from a combination of direct measurement and remotely sensed products over more than a decade and may contain artifacts from the merging of such data.

Synthetic Aperture Radar (SAR)-based velocity observations for the 2008–2009 period [*Joughin et al*., 2010] are nearly complete over the study region and provide the data assimilation target. A small region of the model domain near the divide lacks velocity observations and is filled with balance velocities. We smooth the transition between observational and balance velocity to reduce numerical artifacts during assimilation. The unstructured model mesh is refined following the Hessian of the observed velocity field [*Brinkerhoff and Johnson*, 2013], resulting in mesh spacing ranging from <2 km to 10 km. The final model mesh consists of 10 evenly spaced vertical layers and a total of 31,108 nodal points.

2.5. Model Experimental Design

We perform three different modeling experiments to investigate sensitivity to thermal boundary condition adjustments. Experiment E-REF is forced at the surface and bed by the reference data sets and provides baseline results for comparison. We assimilate surface velocity observations with these thermal boundaries to arrive at a basal traction field and, in order to isolate dynamic effects from boundary condition changes alone, maintain this same traction field through each subsequent experiment. In the second experiment (E-GHF), we keep the reference surface boundary condition constant but change the geothermal heat flux based on available measurements. In the final experiment (E-FULL), both the surface and basal enthalpy boundaries are

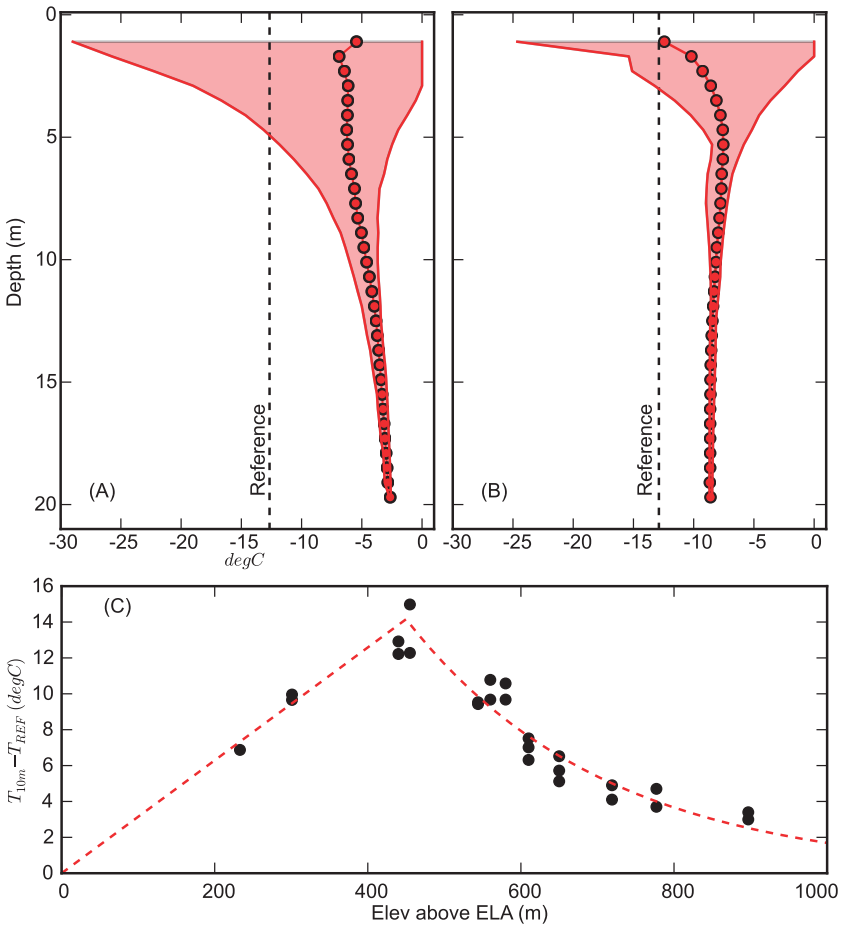

Figure 4. Measured temperatures used to construct the surface temperature field. Ablation zone measurements are shown at sites (a) GL11-S1 and (b) GL11-S2. Red dots show the ablation-corrected mean temperature over the measurement period, bounded by maximum and minimum measurements. Vertical, dashed black line shows the reference surface temperature at the location of the measurements. (c) Difference between 10 m temperatures measured by *Humphrey et al.* [2012] and RACMO surface temperature is shown as a function of elevation above the ELA. Red curve shows the two-part fit we use to scale temperature deviation to our model domain.

adjusted based on measurements. We focus on temperature output from the steady state model as a metric of comparison between these three experiments.

3. Results

3.1. Boundary Conditions

3.1.1. Geothermal Heat Flux

Our interpolated GHF field ranges from 27 mW m^{-2} near the ice sheet margin to 49 mW m^{-2} at the divide (Figure 2). These values are, on average, 23 mW m^{-2} less than the reference field. Our substantially reduced GHF field arises because the GAP borehole site adjacent to the model domain is less than half the value at the equivalent location in the reference data set, and the southern margin measurements are also far lower (Figure 1). While modeled GHF values at GISP and NGRIP are 10 mW m^{-2} higher than the *Shapiro and Ritzwoller* [2004] model, the linearly interpolated field is everywhere lower across the model domain owing to the lower values to the south.

3.1.2. Near-Surface Temperature

Our measurements in the ablation zone show large seasonal variability in temperature in the upper 8 m at both sites and down to ~15 m depth at site GL11-S1 (Figure 4). Temperatures at 20 m depth from both sites show limited fluctuations and are significantly warmer than the reference surface temperatures. At lower site GL11-S1, the difference between measurement and the reference temperature is 10°C. At upper

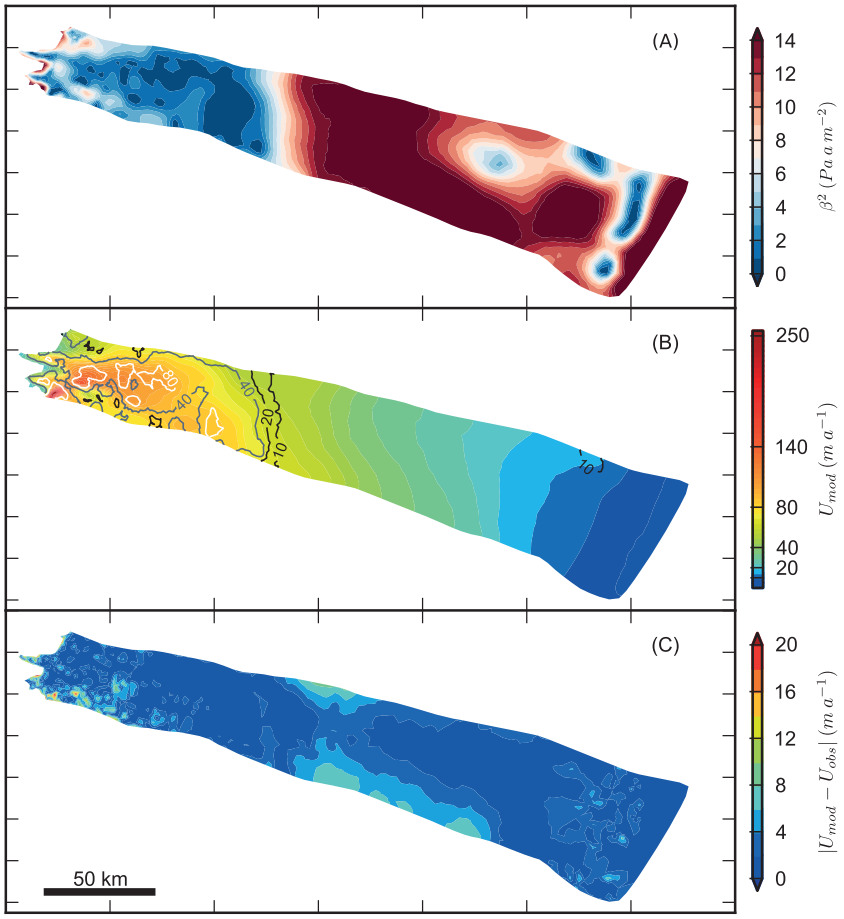

Figure 5. (a) Results from the assimilation procedure to invert for basal traction (β^2). (b) The resulting modeled surface velocity color map, with contours indicating the magnitude of basal sliding in m a^{-1}. (c) The absolute difference between modeled and measured surface velocity.

site GL11-S2 the temperature difference is smaller; 5°C warmer than the reference data set. Near-surface warming in the percolation zone detailed by *Humphrey et al.* [2012] persists when comparing to RACMO surface temperatures. Measured temperatures deviate from the surface reference by up to 15°C (Figure 4). Even at Crawford Point, the highest field site in the *Humphrey et al.* [2012] study, measured temperatures deviate from the reference data set by 3°C. Our observation-constrained field reaches values 14°C warmer than the reference surface temperature and average nearly 6°C warmer over the model domain (Figure 2).

3.2. Modeling

3.2.1. E-REF Results

Results from the assimilation procedure are presented in Figure 5. High-traction values generally limit modeled sliding above the ELA. Exceptions close to the divide correspond to areas where velocity observation uncertainty increases or where balance velocity fills observational gaps. A drop in driving stress from relaxation of surface slopes near the approximate ELA forces a reduction in assimilated basal traction and, correspondingly, a sharp increase in modeled sliding velocity. Maximum surface velocities reach >250 m a^{-1} in the ablation zone but are generally between 90 and 110 m a^{-1}. The resulting RMSE between modeled and observed surface velocities is 3.8 m a^{-1} with a maximum deviation of 27 m a^{-1}.

The basal thermal field under reference boundary conditions shows temperate conditions across nearly the entire model domain (Figures 6a and 7a). At the ice sheet divide basal conditions transition from temperate to -10°C. This variability results from the basal heat flux field, which increases from north to south along the divide (Figure 2), as well as changes in ice thickness, which varies by 300 m. Along the ice sheet margin, a rim of frozen conditions exists where ice is thin and conductive losses are greatest.

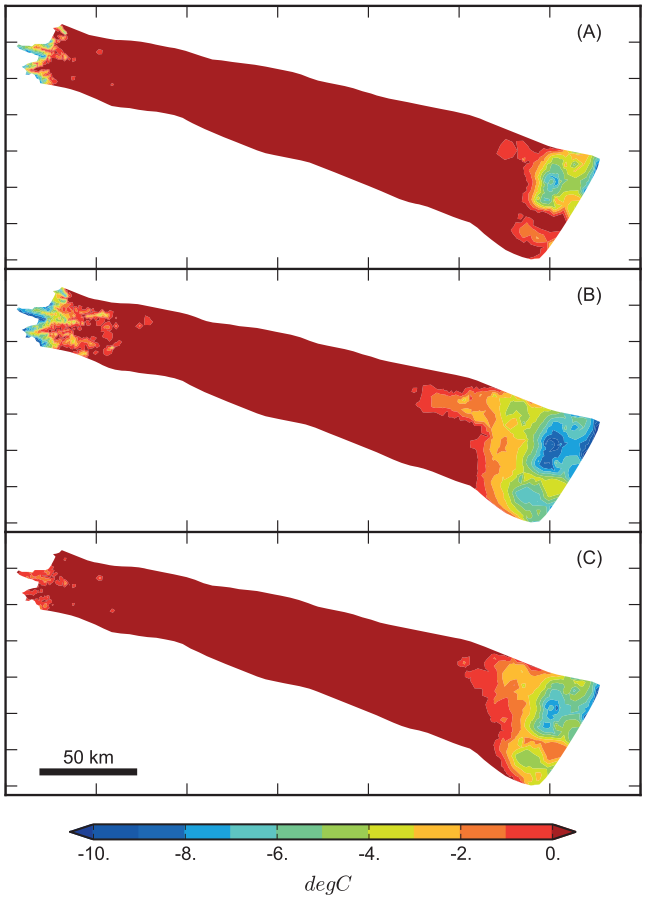

Figure 6. Modeled basal temperature results from the reference case (a) E-REF, (b) E-GHF, and (c) E-FULL with surface and basal boundaries constrained by data. Color bar is consistent across all three panels.

3.2.2. E-GHF Results

Replacing geothermal heat flux with the observation-based field invokes strong changes in the basal thermal regime near the ice sheet divide and margin. Frozen conditions persist along the divide and extend toward the ice sheet margin before modeled basal ice reaches the pressure melting point (Figure 6b). Near the margin, reduced heat flux enlarges the region of frozen conditions compared to E-REF. Basal temperatures below the pressure melting point extend $>$50 km from the ice sheet terminus. The pattern of frozen and temperate conditions is strongly controlled by bedrock topography, with the coldest regions corresponding to topographic highs, and correspondingly thinner ice (Figure 7b).

3.2.3. E-FULL Results

Near the ice sheet divide, the pattern of thermal conditions at the bed resulting from data-driven surface and basal boundary conditions do not differ substantially from E-GHF results (Figure 6c). However, because the imposed surface temperature parameterization scheme generates temperatures at the ice sheet divide slightly warmer than the reference data set ($<$2°C), these warmer temperatures are realized by a slight increase in basal temperatures and corresponding expansion of temperate conditions. Approaching the ice sheet margin, changes in surface temperature invoke significant warming at the bed. Frozen conditions, with temperatures reaching $-$5° to $-$10°C at the bed under E-REF and E-GHF are largely eliminated. A more detailed inspection of the temperatures through the ice column reveals propagation of surface temperature disturbances to depth (Figure 7c). Much of the heat lost through a reduction in basal heat flow appears to be recovered by warming at the surface.

3.3. Comparison Against Measured Temperature Profiles

Our comparisons of model results to measured temperature profiles are not performed with the objective of achieving a perfect match, which would amount to a tuning exercise. Further, a detailed accounting of processes necessary to achieve the measured temperature profiles has been undertaken elsewhere by the authors [*Harrington et al.,* 2015]. Instead, our objective is to use independent measurements through the ice column as an observational benchmark against which biases in modeled thermal conditions can be assessed.

Reference surface boundary temperatures (e.g., E-REF and E-GHF) initiate a modeled cold bias, compared to measurements, that propagates to a depth which is dependent on the prescribed GHF (Figure 8). The cold bias is eliminated by the bed under the reference GHF (E-REF). All boreholes which reached the bed (GL11-S1, GL12-S2, GL11-S2) indicate temperate basal conditions which are also reproduced by E-REF. In contrast, the model cold bias propagates through the entire ice column under reduced GHF based on observations. The cold bias under E-GHF reaches $-$7°C in the ice column, and basal temperatures reach values colder than $-$3°C at measurement sites.

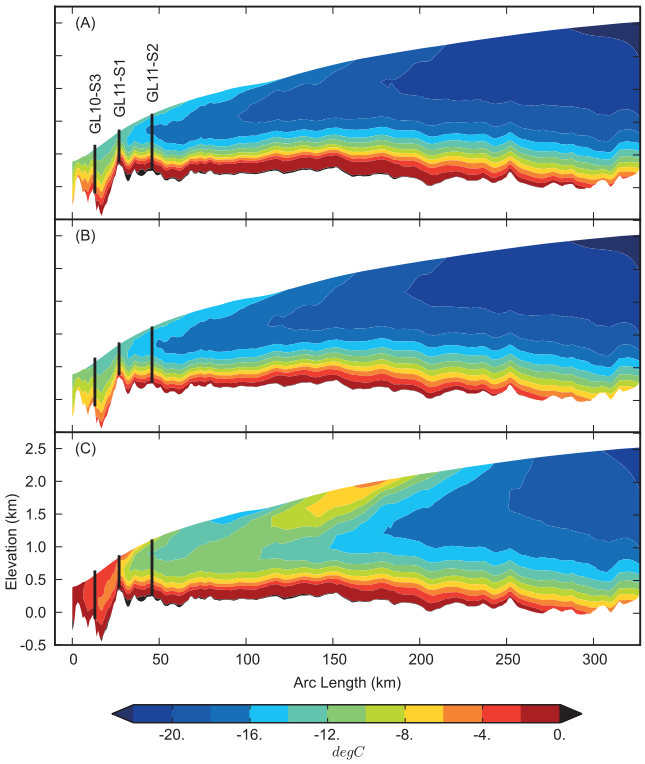

Figure 7. Temperature fields along a transect (see Figure 1) resulting from (a) E-REF, (b) E-GHF, and (c) E-FULL. The color bar is consistent for each panel. Vertical bars denote locations, surface elevations, and bed elevations of boreholes shown in Figure 1.

The observation-based surface temperature parameterization under E-FULL has a large impact on temperatures through the ablation zone. In the upper half of the ice column the warmer surface condition generates a closer fit to measurements, although modeled ice temperatures generally remain colder than measured. In the lower half of the ice column, results are mixed. Model temperatures are nearly 3°C warmer than measurements

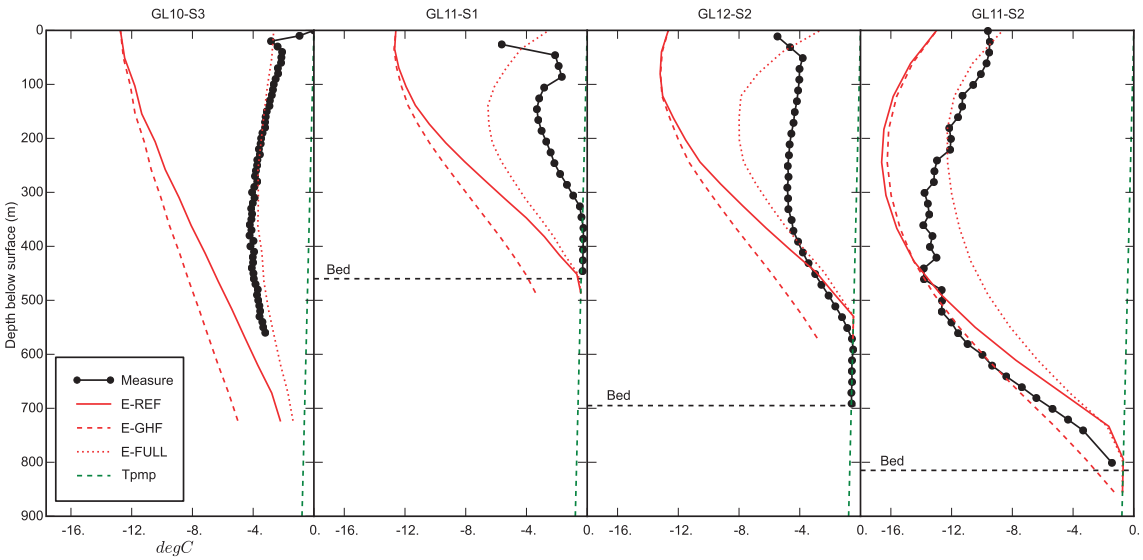

Figure 8. Measured and modeled temperatures at four sites in the ablation zone (see Figure 1). Modeled temperatures from E-REF, E-GHF, and E-FULL are shown as solid, dashed, and dotted red lines, respectively. Measured depth to the ice sheet bed during drilling is indicated by the horizontal, dashed black line (the bed was not reached in hole GL10-S3). The approximate pressure melting temperature is shown as the dashed green line.

at GL11-S2 but remain too cold at GL11-S1. The modeled E-FULL temperature curve near the bed is quite similar to that from E-REF, despite significantly reduced basal heat flux. Compared to E-GHF, ice temperatures at each of the measurement sites are warmer by at least 3°C through the ice column.

4. Discussion

4.1. Assumptions and Limitations

Our linearly interpolated GHF field is strongly controlled by a single heat flux measurement within our model domain and utilizes measurements hundreds of kilometers from the study area. Spatially variable basal melt rates elsewhere on the ice sheet suggest correspondingly heterogeneous basal heat flux [*Buchardt and Dahl-Jensen*, 2007]. Such spatial complexity may result from variations in radioactive decay in the Earth's crust [*Näslund et al*., 2005]. As a result, our linear interpolation technique may be a simplification of the real-world heat fluxes beneath the ice sheet, emphasizing measurements that could be spatially anomalous. However, other anecdotal evidence exists which supports the low GHF values we prescribe. While recent conclusions have suggested a thin lithosphere in central and northern GrIS [*Petrunin et al*., 2013], interpretations of *S* receiver functions suggest increasing lithosphere thickness by up to 50% further south on the ice sheet, as well as from east to west [*Kumar et al*., 2005]. Rayleigh wave tomography supports the east-to-west thickening of old, stable lithosphere in the southern portion of the ice sheet [*Darbyshire et al*., 2004]. Previous work suggests a close relationship between lithosphere thickness and Curie depth (depth of 580°C isotherm) [*Negi et al*., 1987; *Petrunin et al*., 2013], with an associated influence on the thermal gradient and hence heat flux. Additional evidence for decreased GHF values in southern GrIS stems from previous ice sheet modeling by *Greve* [2005], who found it necessary to reduce GHF to 20 mW m^{-2} at the Dye 3 site in order to fit the modeled basal temperature to that measured in the ice core. The latter study supports our low GHF, but this result is not included in our measurement-driven field because of compounding uncertainty of past temperatures and precipitation rates on fitting Dye 3 basal conditions [*Dahl-Jensen et al*., 1998; *Rogozhina et al*., 2012].

The discrepancy between mean annual surface temperature from the reference RCM and near-surface measurements demonstrates that a more plausible surface boundary—one that incorporates warming effects from meltwater refreezing and water-filled features near the surface, should be used to constrain flow models. Yet our observations of near-surface temperature are limited in both space and time. In the ablation zone, the presence of crevasses and moulins could induce a spatially complex thermal field near the surface that is not appropriately reflected by our parameterization. The short measurement duration also presents a conflict of time scales, as advection of near-surface temperatures to depths of a few hundred meters requires centuries in the model. This suggests that the surface boundary in a steady state model may be more appropriately reflected by near-surface warming effects that are time-averaged over a longer period than our snapshots.

Interpretation of any model results hinges on assumptions and limitations within the numerical model. As detailed above, our assumption of steady state and neglect of historical climate change is a significant but necessary constraint under the current assimilation method. Modeled vertical velocities impose a control on heat advection and are influenced by uncertainties in bedrock topography and by the fact that we do not explicitly account for melting at the basal boundary [*Brinkerhoff and Johnson*, 2013]. Other uncertainties in the modeling experiments are present in the description of deformation, where we assume a stress exponent of $n = 3$ and have not prescribed enhanced deformation.

The combined effect of these limitations may lead to a flow field and thermal profile which are inconsistent with present-day observations. Unfortunately, many of the limitations described above are common to all numerical ice sheet models. Realistic treatment of processes relating to the constitutive law for ice requires in situ measurements which are rare. While we neglect basal melting in vertical velocity calculations, modeled melt rates in excess of 2 cm a^{-1} are scarce and second-order compared to the influence of basal topography on vertical flow. In the ablation zone gradients in bed topography, which is constrained by dense airborne radar in our study area, induce vertical velocities on the order of 10 m a^{-1}. Vertical flow of this magnitude is localized but interpretation of modeled results must bear this limitation in mind. A glacial spin-up may alleviate the steady state assumption but introduces new uncertainties regarding temporal changes in basal sliding and historical climate. In sum, we acknowledge the limitations of our numerical study but assert that the modeling tools are commensurate with the current state of the art in ice sheet modeling practice.

4.2. Boundary Condition Impacts on Numerical Modeling

Previous research has documented the importance of reducing GHF, compared to standard data sets, in southern GrIS in order to improve the misfit between measured and modeled temperatures at the ice divide [*Greve*, 2005; *Rogozhina et al*., 2012]. While our lower, measurement-based GHF field is in agreement with these studies, our modeling results honoring reduced basal heat flux generate fast sliding over a frozen bed in the ablation zone which is physically untenable. Small amounts of cold-based sliding (10^{-4}–10^{-1} m a^{-1}) have been previously observed at glacier and ice sheet margins [*Echelmeyer and Zhongxiang*, 1987; *Cuffey et al*., 1999], but slip rates of tens of m a^{-1} over a frozen bed in E-GHF are not likely realistic. Further, nearby observations of subglacial water issuing from the ice sheet margin [*Bartholomew et al*., 2011] indicate temperate basal conditions at least dominate in the lower ablation zone. Direct temperature measurement in our boreholes shows that anomalously cold conditions are not limited to the bed but are pervasive through the ice column under E-GHF (Figure 8). Clearly, the lower basal heat flux necessary to improve model behavior close to the divide has the opposite effect near the ice sheet margin, suggesting one or more heat sources are missing in the E-GHF model formulation.

Despite maintaining a constant basal traction field in experiments, discrepancies in sliding velocities between E-GHF and E-REF exist and could cause discrepancies in frictional heat generation that influence the basal thermal regime. Sliding velocity differences between the two experiments are generally <5 m a^{-1} but locally reach values of 18 m a^{-1}. However, deviations of this magnitude are sparse and concentrated in regions where basal traction is low. Because the frictional heat generated from sliding is dependent on the basal traction field (equation (1)), the change in frictional heat associated with lower sliding in E-GHF amounts to no more than 5 mW m^{-2}, and is <1 mW m^{-2} over the vast majority of the domain. We thus conclude that the change in sliding velocities between E-REF and E-GHF is insufficient to account for the heat lost from lowering GHF.

The importance of meltwater as an agent for changing the thermal structure of the GrIS in the ablation zone is becoming increasingly appreciated. The frictional dissipation of heat from water flowing through an active basal drainage system provides a heat source at the ice/bedrock surface but is limited to the basal plane. Warming from water-filled features extending through the full ice thickness, such as moulins or crevasses, has been demonstrated to be sufficient to match temperature profiles to the north along the EGIG line [*Phillips et al*., 2010]. In our study area, local modeling suggests meltwater-driven thermal perturbations can influence the thermal structure near the surface, bed, and within the column as a result of surface crevasses, basal crevasses, and moulins, respectively [*Harrington et al*., 2015]. Yet unfortunately, the degree of warming induced by these macroscale features is dependent on their spatial distribution, water-filled state, and depth of propagation. Difficulties in constraining the density and vertical extent of these features hinder quantification of their warming influence across the ablation zone.

In addition to thermal effects from discrete hydrologic features, our results show that adjustment of the near-surface boundary in accordance with measurements drives large-scale changes of the thermal structure toward the ice sheet margin. As a result, warming near the surface alone is sufficient to overcome a substantial portion of the apparent cold bias generated from model-based surface temperatures and reduced basal heat flux. In particular, temperature adjustments in the percolation zone propagate to depth, and while they do not have an impact on the already temperate basal conditions above the ELA, conductive heating reduces the cold temperatures from deeper in the ice sheet interior. The integrated effect of this warming is realized in the ablation zone, where strong temperature gradients in thinner ice are reduced, and the destruction of the interior cold plug limits advective effects from ice flow around complex basal topography. Sensitivity testing over a range of surface temperature perturbations shows an approximately linear relationship between the magnitude of perturbation and the resulting area of frozen bed conditions in the ablation zone. Thus, even small deviations from standard, model-based surface temperature data sets have a measurable impact on modeled basal conditions.

Our results reveal that the surface boundary condition is a key component of the modeled thermal budget. The importance of this boundary is likely to be magnified in the southern portion of the GrIS where there is evidence for reduced heat flux from below, and surface melting effects are amplified compared to elsewhere on the GrIS. Model simulations show that, integrated across the domain, the additional energy from surface boundary changes is over 3 times larger than the energy lost from reduced basal heat flux. As highlighted by the recent discovery of perennial liquid water under cold conditions in the percolation zone [*Forster et al*., 2014],

significant limitations remain with respect to our understanding of meltwater generation and routing processes on the ice sheet. Thermal effects do not appear to be limited to shallow depths, implying that, in addition to influencing mass balance uncertainties [*Harper et al*., 2012], meltwater storage and refreezing may also be an important contributing factor to the ice sheet thermal profile, albeit given sufficient time scales.

5. Conclusions

In this study we have combined measurements near the ice sheet surface, below the ice sheet bed, and within the ice column to develop new observationally constrained thermal boundary conditions for western GrIS. We assess the subsequent impact of these new fields on the modeled thermal regime of the ice sheet as compared to prior existing and commonly used data sets. Our measurement-based boundaries prescribe low basal heat flux and high near-surface temperatures relative to commonly used fields. Near-surface temperatures in both the percolation and ablation zones are measured to be up to 15°C warmer than equivalent reference output. Conversely, existing observations indicate geothermal heat flux 30 mW m^{-2} less than is commonly prescribed; a reduction of more than 50%.

The realization of boundary condition discrepancies between measurements and spatially distributed data sets in a higher-order ice flow model indicates that the boundary conditions are first-order drivers of the ice sheet thermal profile. Reduction of geothermal heat flux alone commensurate with observations increases the modeled cold bias compared to measured temperature profiles and expands the region of frozen basal conditions through the ablation zone. When including observation-based conditions near the surface, temperate bed conditions dominate in the ablation zone and the cold bias higher in the ice column is reduced. The thermal surface boundary must therefore be carefully treated in thermomechanically coupled model experiments.

The future dynamical behavior of the Greenland Ice Sheet remains poorly constrained, due in part to a limited understanding of the expected basal sliding response to climate changes. In the absence of a universal sliding law, sliding sensitivity experiments, whereby initial sliding conditions are multiplied by a constant amplification factor, have yielded an envelope of potential ice sheet dynamical behavior [*Bindschadler et al*., 2013; *Nowicki et al*., 2013]. Model-based tuning of basal traction to match observed velocities is prone to thermally induced biases which influence internal deformation, and hence sliding/deformational velocity partitioning. Our results indicate that the surface and basal boundary conditions critically dictate thermal behavior through the full ice thickness, necessitating careful consideration during such model initialization. Cold model conditions from inadequate treatment of the near-surface layer may thus be manifested in the velocity regime through enhanced sliding, which is amplified in modeled future ice sheet behavior when this initial sliding condition is perturbed.

Acknowledgments

This work is funded by SKB-Posiva-NWMO through the Greenland Analogue Project, NSF (Office of Polar Programs-Arctic Natural Sciences grant 0909495), and NASA grant NNX11AM12A. We thank L. Claesson Liljedahl and J.O. Näslund for their careful critiques which substantially improved an earlier version of the manuscript. Comments from three anonymous reviewers added greatly to the manuscript. Data sets are published by the Swedish Nuclear Waste Management Company at the following web address: http://www.skb.se/Templates/Standard__17139.aspx.

References

Allen, C., C. Leuschen, P. Gogineni, F. Rodriguez-Morales, and J. Paden (2010), IceBridge MCoRDS L2 Ice Thickness, NASA DAAC at the Natl. Snow and Ice Data Cent., Boulder, Colo. [Updated 2014.]

Aschwanden, A., E. Bueler, C. Khroulev, and H. Blatter (2012), An enthalpy formulation for glaciers and ice sheets, *J. Glaciol*., *58*(209), 441–457, doi:10.3189/2012JoG11J088.

Aster, R. C., B. Borhers, and C. H. Thurber (2005), *Parameter Estimation and Inverse Problems*, Elsevier Acad. Press, San Diego, Calif.

Bamber, J. L., et al. (2013), A new bed elevation dataset for Greenland, *Cryosphere*, *7*(2), 499–510, doi:10.5194/tc-7-499-2013.

Bartholomew, I., P. Nienow, A. Sole, D. Mair, T. Cowton, S. Palmer, and J. Wadham (2011), Supraglacial forcing of subglacial drainage in the ablation zone of the Greenland Ice Sheet, *Geophys. Res. Lett*., *38*, L08502, doi:10.1029/2011GL047063.

Benson, C. S. (1962), Stratigraphic studies in the snow and firn of the Greenland Ice Sheet, *Res. Rep. 70*, 120 pp., Snow, Ice and Permafrost Res. Estab., U. S. Army Corps of Eng., Hanover, N.H.

Bindschadler, R. A., et al. (2013), Ice-sheet model sensitivities to environmental forcing and their use in projecting future sea level (the SeaRISE project), *J. Glaciol*., *59*(214), 195–224, doi:10.3189/2013JoG12J125.

Blatter, H. (1995), Velocity and stress fields in grounded glaciers: A simple algorithm for including deviatoric stress gradients, *J. Glaciol*., *41*(138), 333–344.

Box, J. E., D. H. Bromwich, B. A. Veenhuis, L. S. Bai, J. C. Stroeve, J. C. Rogers, K. Steffen, T. Haran, and S. H. Wang (2006), Greenland Ice Sheet surface mass balance variability (1988–2004) from calibrated polar MM5 output, *J. Clim*., *19*, 2783–2800.

Brinkerhoff, D. J., and J. V. Johnson (2013), Data assimilation and prognostic whole ice sheet modelling with the variationally derived, higher order, open source, and fully parallel ice sheet model VarGlaS, *Cryosphere*, *7*(4), 1161–1184, doi:10.5194/tc-7-1161-2013.

Buchardt, S. L., and D. Dahl-Jensen (2007), Estimating the basal melt rate at NorthGRIP using a Monte Carlo technique, *Ann. Glaciol*., *45*(1), 137–142, doi:10.3189/172756407782282435.

Cuffey, K. M., and W. S. B. Patterson (2010), *The Physics of Glaciers*, 4th ed., Elsevier, Oxford, U. K.

Cuffey, K. M., H. Conway, B. Hallet, A. M. Gades, and C. F. Raymond (1999), Interfacial water in polar glaciers and glacier sliding at −17 °C, *Geophys. Res. Lett*., *26*(6), 751–754, doi:10.1029/1999GL900096.

Dahl-Jensen, D., K. Mosegaard, N. Gundestrup, G. D. Clow, S. J. Johnsen, A. W. Hansen, and N. Balling (1998), Past temperatures directly from the Greenland Ice Sheet, *Science*, *282*(5387), 268–271, doi:10.1126/science.282.5387.268.

Darbyshire, F. A., T. B. Larsen, K. Mosegaard, T. Dahl-Jensen, Ó. Gudmundsson, T. Bach, S. Gregersen, H. A. Pedersen, and W. Hanka (2004), A first detailed look at the Greenland lithosphere and upper mantle, using Rayleigh wave tomography, *Geophys. J. Int.*, *158*(1), 267–286, doi:10.1111/j.1365-246X.2004.02316.x.

Echelmeyer, K., and W. Zhongxiang (1987), Direct observation of basal sliding and deformation of basal drift at sub-freezing temperatures, *J. Glaciol.*, *33*(113), 83–98.

Echelmeyer, K., W. D. Harrison, T. S. Clarke, and C. Benson (1992), Surficial glaciology of Jakobshavns Isbrae, west Greenland: Part II. Ablation, accumulation and temperature, *J. Glaciol.*, *38*(128), 169–181.

Ettema, J., M. R. van den Broeke, E. van Meijgaard, W. J. van de Berg, J. L. Bamber, J. E. Box, and R. C. Bales (2009), Higher surface mass balance of the Greenland Ice Sheet revealed by high-resolution climate modeling, *Geophys. Res. Lett.*, *36*, L12501, doi:10.1029/2009GL038110.

Forster, R. R., et al. (2014), Extensive liquid meltwater storage in firn within the Greenland Ice Sheet, *Nat. Geosci.*, *7*, 95–98, doi:10.1038/ngeo2043.

Fox Maule, C., M. E. Purucker, and N. Olsen (2009), Danish Climate Centre Report 09–09 Inferring magnetic crustal thickness and geothermal heat flux from crustal magnetic field models.

Gillet-Chaulet, F., O. Gagliardini, H. Seddik, M. Nodet, G. Durand, C. Ritz, T. Zwinger, R. Greve, and D. G. Vaughan (2012), Greenland Ice Sheet contribution to sea-level rise from a new-generation ice-sheet model, *Cryosphere*, *6*(6), 1561–1576, doi:10.5194/tc-6-1561-2012.

Greve, R. (2005), Relation of measured basal temperatures and the spatial distribution of the geothermal heat flux for the Greenland Ice Sheet, *Ann. Glaciol.*, *42*(1), 424–432, doi:10.3189/172756405781812510.

Habermann, M., D. Maxwell, and M. Truffer (2012), Reconstruction of basal properties in ice sheets using iterative inverse methods, *J. Glaciol.*, *58*(210), 795–807, doi:10.3189/2012JoG11J168.

Harrington, J. A., N. F. Humphrey, and J. T. Harper (2015), Temperature distribution and thermal anomalies along a flowline of the Greenland Ice Sheet, *Ann. Glaciol.*, *56*(70), 70A945, in press.

Harper, J., et al. (2010), The Greenland Analogue Project Yearly Report 2010, R-11-23, Svensk Karnbranslehanterin AB.

Harper, J., N. Humphrey, W. T. Pfeffer, J. Brown, and X. Fettweis (2012), Greenland Ice-Sheet contribution to sea-level rise buffered by meltwater storage in firn, *Nature*, *491*(7423), 240–243, doi:10.1038/nature11566.

Hooke, R. L., J. E. Gould, and J. Brzozowski (1983), Near-surface temperatures near and below the equilibrium line on polar and subpolar glaciers, *Z. Gletscherkd. Glazialgeol.*, *19*(1), 1–25.

Humphrey, N. F., J. T. Harper, and W. T. Pfeffer (2012), Thermal tracking of meltwater retention in Greenland's accumulation area, *J. Geophys. Res.*, *117*, F01010, doi:10.1029/2011JF002083.

Jarvis, G. T., and G. K. C. Clarke (1974), Thermal effects of crevassing on Steele Glacier, Yukon Territory, Canada, *J. Glaciol.*, *13*(68), 243–254.

Joughin, I., B. E. Smith, I. M. Howat, T. Scambos, and T. Moon (2010), Greenland flow variability from ice-sheet-wide velocity mapping, *J. Glaciol.*, *56*(197), 415–430, doi:10.3189/002214310792447734.

Koenig, L. S., C. Miège, R. R. Forster, and L. Brucker (2014), Initial in situ measurements of perennial meltwater storage in the Greenland firn aquifer, *Geophys. Res. Lett.*, *41*, 81–85, doi:10.1002/2013GL058083.

Kumar, P., et al. (2005), The lithosphere–asthenosphere boundary in the North-West Atlantic region, *Earth Planet. Sci. Lett.*, *236*, 249–257, doi:10.1016/j.epsl.2005.05.029.

Larour, E., H. Seroussi, M. Morlighem, and E. Rignot (2012), Continental scale, high order, high spatial resolution, ice sheet modeling using the Ice Sheet System Model (ISSM), *J. Geophys. Res.*, *117*, F01022, doi:10.1029/2011JF002140.

Meierbachtol, T., J. Harper, and N. Humphrey (2013), Basal drainage system response to increasing surface melt on the Greenland Ice Sheet, *Science*, *341*(6147), 777–779, doi:10.1126/science.1235905.

Mock, S. J., and W. F. Weeks (1965), The distribution of 10 meter snow temperatures on the Greenland Ice Sheet, *J. Glaciol.*, *6*, 23–41.

Näslund, J.-O., P. Jansson, J. L. Fastook, J. Johnson, and L. Andersson (2005), Detailed spatially distributed geothermal heat-flow data for modeling of basal temperatures and meltwater production beneath the Fennoscandian Ice Sheet, *Ann. Glaciol.*, *40*(1), 95–101, doi:10.3189/172756405781813582.

Negi, J. G., P. K. Agrawal, and P. Pandey (1987), Large variation of Curie depth and lithospheric thickness beneath the Indian subcontinent and a case for magnetothermometry, *Geophys. J. R. Astron. Soc.*, *88*, 763–775.

Nocedal, J., and S. J. Wright (2000), in *Numerical Optimization*, 2nd ed., edited by T. V. Mikosch, S. M. Robinson, and S. I. Resnick, Springer, New York.

Nowicki, S., et al. (2013), Insights into spatial sensitivities of ice mass response to environmental change from the SeaRISE ice sheet modeling project II: Greenland, *J. Geophys. Res. Earth Surf.*, *118*, 1025–1044, doi:10.1002/jgrf.20076.

Pattyn, F. (2003), A new three-dimensional higher-order thermomechanical ice sheet model: Basic sensitivity, ice stream development, and ice flow across subglacial lakes, *J. Geophys. Res.*, *108*(B8), 2382, doi:10.1029/2002JB002329.

Petrunin, A. G., I. Rogozhina, A. P. M. Vaughan, I. T. Kukkonen, M. K. Kaban, I. Koulakov, and M. Thomas (2013), Heat flux variations beneath central Greenland's ice due to anomalously thin lithosphere, *Nat. Geosci.*, *6*(8), 746–750, doi:10.1038/ngeo1898.

Pfeffer, W. T., and C. S. Bretherton (1987), The effect of crevasses on the solar heating of a glacier surface, *Phys. Basis Ice Sheet Modell.*, *170*, 191–205.

Phillips, T., H. Rajaram, and K. Steffen (2010), Cryo-hydrologic warming: A potential mechanism for rapid thermal response of ice sheets, *Geophys. Res. Lett.*, *37*, L20503, doi:10.1029/2010GL044397.

Pollack, H. N., S. J. Hurter, and R. Johnson (1993), Heat flow from the Earth's interior: Analysis of the global data set, *Rev. Geophys.*, *31*(3), 267–280, doi:10.1029/93RG01249.

Reeh, N. (1991), Parameterization of melt rate and surface temperature on the Greenland Ice Sheet, *Polarforschung*, *5913*, 113–128.

Rignot, E., and J. Mouginot (2012), Ice flow in Greenland for the International Polar Year 2008–2009, *Geophys. Res. Lett.*, *39*, L11501, doi:10.1029/2012GL051634.

Rogozhina, I., J. M. Hagedoorn, Z. Martinec, K. Fleming, O. Soucek, R. Greve, and M. Thomas (2012), Effects of uncertainties in the geothermal heat flux distribution on the Greenland Ice Sheet: An assessment of existing heat flow models, *J. Geophys. Res.*, *117*, F02025, doi:10.1029/2011JF002098.

Sass, J. H., B. L. Nielsen, H. A. Wollenberg, and R. J. Munroe (1972), Heat flow and surface radioactivity at two sites in south Greenland, *J. Geophys. Res.*, *77*(32), 6435–6444, doi:10.1029/JB077i032p06435.

Seroussi, H., M. Morlighem, E. Rignot, A. Khazendar, E. Larour, and J. Mouginot (2013), Dependence of century-scale projections of the Greenland Ice Sheet on its thermal regime, *J. Glaciol.*, *59*(218), 1024–1034, doi:10.3189/2013JoG13J054.

Shapiro, N. M., and M. H. Ritzwoller (2004), Inferring surface heat flux distributions guided by a global seismic model: Particular application to Antarctica, *Earth Planet. Sci. Lett.*, *223*, 213–224, doi:10.1016/j.epsl.2004.04.011.

Steffen, K., J. E. Box, and W. Abdalati (1996), Greenland Climate Network: GC-Net, in *CRREL 96–27 Spec. Rep. Glaciers, Ice Sheets Volcanoes, Trib. to M. Meier*, pp. 98–103.

Van de Wal, R. S. W., W. Boot, M. R. van den Broeke, C. J. P. P. Smeets, C. H. Reijmer, J. J. A. Donker, and J. Oerlemans (2008), Large and rapid melt-induced velocity changes in the ablation zone of the Greenland Ice Sheet, *Science*, *321*(5885), 111–113, doi:10.1126/science.1158540.